

Measurement cost of metric-aware variational quantum algorithms

Barnaby van Straaten and Bálint Koczor*

Department of Materials, University of Oxford, Parks Road, Oxford OX1 3PH, United Kingdom

Variational quantum algorithms are promising tools for near-term quantum computers as their shallow circuits are resilient to experimental imperfections. Their practical applicability, however, strongly depends on how many their circuits need to be repeated for sufficiently reducing shot-noise. We consider metric-aware quantum algorithms: variational algorithms that use a quantum computer to efficiently estimate both a matrix and a vector object. For example, the recently introduced quantum natural gradient approach uses the quantum Fisher information matrix as a metric tensor to correct the gradient vector for the co-dependence of the circuit parameters. We rigorously characterise and upper bound the number of measurements required to determine an iteration step to a fixed precision, and propose a general approach for optimally distributing samples between matrix and vector entries. Finally, we establish that the number of circuit repetitions needed for estimating the quantum Fisher information matrix is asymptotically negligible for an increasing number of iterations and qubits.

With quantum computers rising as realistic technologies, attention has turned to how such machines could perform as variational tools [1–20]. This results in a hybrid model with an iterative loop: a classical processor determines how to update the parameters describing a family of quantum states (parametrised ansatz states), while a quantum coprocessor generates and performs measurements on that state (via an ansatz circuit). This is of particular interest in the context of noisy, intermediate-scale quantum devices (NISQ devices) [21], because complex ansatz states can be prepared with shallow circuits [22–25], potentially obtaining useful value before the era of resource-intensive quantum fault tolerance methods.

Attention has recently been focused on statistical aspects of these variational quantum algorithms [26–30], such as the effect of shot noise and the reduction of their measurement costs. It is our aim in this work to establish general scaling results by rigorously characterising the number of measurements required to obtain a single iteration step in case of so-called metric-aware quantum algorithms. Let us first introduce basic notions.

Variational quantum algorithms — We consider variational quantum algorithms which typically aim to prepare a parametrised quantum state $\rho(\underline{\theta}) := \Phi(\underline{\theta})\rho_0$ where we model via a mapping $\Phi(\underline{\theta})$ that acts on the computational zero state ρ_0 of N qubits and depends continuously on the parameters θ_i with $i = \{1, 2, \dots, \nu\}$. This mapping can in general contain non-unitary elements, such as measurements [31], but in many applications one assumes that it acts (approximately) as a unitary circuit that decomposes into a product of individual quantum gates. These gates typically act on a small subset of the system, e.g., one and two-qubit gates. The benefit of this construction is that the number of parameters ν only grows polynomially with the number of qubits; therefore the iterative parameter update rules are classically tractable.

Recently a novel variational algorithm was proposed for simulating real-time quantum evolution using shallow quantum circuits [8] introducing a novel feature: a matrix object that characterises the sensitivity of the ansatz state $\rho(\underline{\theta})$ to changes in each possible pair of parameters, but without reference to the cost function. This approach was further generalised to imaginary time and natural gradient evolutions [31, 32] which can be used as optimisers of variational quantum eigensolvers (VQE) [2, 4, 33]. This was shown to significantly outperform other approaches, such as simple gradient descent, in terms of convergence speed and accuracy according to numerical simulations [31, 32, 34].

In this work, we consider generalisations of the aforementioned techniques as variational algorithms that depend on both a positive-semidefinite, symmetric matrix – a metric tensor that characterises sensitivity with respect to parameters θ_k – and on a vector object. Many examples of such algorithms are provided in references [31, 32, 35–37], and we will refer to them in the following as metric-aware quantum algorithms. The metric tensor typically only depends on the parameter values while the vector object additionally depends on, e.g., a Hermitian observable \mathcal{H} – and \mathcal{H} decomposes into a polynomially increasing number r_h of Pauli terms.

Quantum natural gradient — To be more concrete, in the following we will focus on one prominent algorithm, the recently introduced quantum natural gradient approach [31, 37] which is equivalent to imaginary time evolution when quantum circuits are noiseless and unitary [31, 32]. This approach can be used as a VQE optimiser when minimising the expectation value $E(\underline{\theta}) := \text{Tr}[\rho(\underline{\theta})\mathcal{H}]$ over the parameters $\underline{\theta}$. However, the approach generalises to any Lipschitz continuous mapping as an objective function.

In particular, natural gradient descent governs the evolution of the ansatz parameters according to the update rule [31]

$$\underline{\theta}(t+1) = \underline{\theta}(t) - \lambda \mathbf{F}_Q^{-1} \underline{g}, \quad (1)$$

where t is an index and λ is a step size. Here the inverse

* balint.koczor@materials.ox.ac.uk

of the positive-semidefinite, symmetric quantum Fisher information matrix $\mathbf{F}_Q \in \mathbb{R}^{\nu \times \nu}$ corrects the gradient vector $g_k := \partial_k E(\theta)$ for the co-dependence of the parameters, and both objects can be estimated efficiently using a quantum computer while the inverse \mathbf{F}_Q^{-1} is computed by a classical processor. Note that the introduction of the matrix \mathbf{F}_Q as a metric tensor accelerates the convergence speed of the simple gradient descent approach [31, 32, 34], as the latter corresponds to the possible special case $\mathbf{F}_Q = \text{Id}_\nu$ of the former.

We discuss different protocols for estimating the matrix $[\mathbf{F}_Q]_{kl}$ and vector g_k entries for both pure (idealised, perfect quantum gates) and mixed quantum states (via imperfect quantum gates or non-unitary elements as measurements) in the Appendix. We now highlight two results. a) We derive the general upper bound $[\mathbf{F}_Q]_{kl} \leq r_g^2$, where r_g is the maximal Pauli rank of the ansatz gates in case of unitary parametrisations (Lemma 1). This bound is a generalisation of what is known as the Heisenberg limit in quantum metrology [38], refer also to [39–41]. We remark that in practice this Pauli rank r_g is a small constant. For example, even the choice $r_g = 1$ includes universal quantum circuits composed of single qubit X , Y and Z rotations as well as two-qubit XX , YY and ZZ gates. b) The matrix \mathbf{F}_Q might be ill-conditioned and the inversion in Eq. 1 requires a regularisation. We will use the simple variant of Tikhonov regularisation $\mathbf{F}_Q^{-1} := [\mathbf{F}_Q + \eta \text{Id}]^{-1}$ in the following; we derive analytical lower and upper bounds on the singular values of this inverse matrix in the Appendix (Lemma 3) using a).

Upper bounds on the measurement cost — Equipped with basic notions we now focus on quantifying the measurement cost of these variational algorithms. To motivate our approach, we illustrate in Fig 1 (a/green) how naively using the same number of measurements for estimating each matrix and vector entry, such as in [34], can result in impractical sampling costs.

In particular, we aim to reduce the error ϵ of the vector $\underline{v} := \mathbf{F}_Q^{-1} \underline{g}$ in the update rule in Eq. (1). We first express how the error due to finite sampling of the matrix and vector entries propagates to the parameter-update rule in Eq. (1). We quantify this error as the expected Euclidean distance $\langle \|\Delta v\|^2 \rangle = \epsilon^2$, and this translates to the condition $\sum_{k=1}^{\nu} \text{Var}[v_k] = \epsilon^2$, where $\text{Var}[v_k]$ is the variance of a single vector entry. In practice this precision can be either a fixed parameter or could be adapted throughout the evolution as, e.g., $\epsilon = \|v(t)\|$ where t is an index.

We derive an analytical formula in Lemma 2 in the Appendix: we express the error ϵ in terms of the variances $\text{Var}\{[\mathbf{F}_Q]_{kl}\}$ and $\text{Var}[g_k]$ of the measurements used to estimate the matrix and vector entries, respectively, as

$$\epsilon^2 = \sum_{k,l=1}^{\nu} a_{kl} \text{Var}\{[\mathbf{F}_Q]_{kl}\} + \sum_{k=1}^{\nu} b_k \text{Var}[g_k]. \quad (2)$$

The coefficients a_{kl} describe how the error of $[\mathbf{F}_Q]_{kl}$ propagates through matrix inversion and subsequent vector

multiplication into the precision ϵ . Likewise b_k describes how errors in the estimated vector propagate through the multiplication $\mathbf{F}_Q^{-1} \underline{g}$. In both cases a large coefficient indicates that the vector \underline{v} is particularly sensitive to errors in estimating the corresponding matrix or vector element. We remark that these results are completely general and can be applied to any quantum algorithm that requires the estimation of both an inverse matrix and a vector object.

We derive general upper bounds on the variances $\text{Var}\{[\mathbf{F}_Q]_{kl}\}$ and $\text{Var}[g_k]$ for different experimental strategies in the Appendix; The error ϵ^2 in Eq. 2 is reduced proportionally when repeating measurements. In the following, we assume that N_F measurements are assigned to estimate the full matrix \mathbf{F}_Q while N_g measurements are used to estimate the gradient vector \underline{g} . We now state an upper bound on them in terms of the precision ϵ .

Theorem 1. *To reduce the uncertainty of the vector $\underline{v} = \mathbf{F}_Q^{-1} \underline{g}$ due to shot noise to a precision ϵ , the number of samples to estimate the matrix \mathbf{F}_Q in Eq. (1) is upper bounded as*

$$N_F \leq 2\epsilon^{-2} \nu^4 \text{Spc}[\mathbf{F}_Q^{-1}]^2 \|g\|_{\infty}^2 f_F \quad (3)$$

while sampling the gradient has a cost upper bounded by

$$N_g \leq 2\epsilon^{-2} \nu^2 \text{Spc}[\mathbf{F}_Q^{-1}] \text{Spc}[\mathcal{H}] f_g. \quad (4)$$

The overall measurement cost of determining the natural gradient vector is $N_F + N_g$. Here $\text{Spc}[A]$ denotes the average squared singular values of a matrix $A \in \mathbb{C}^{d \times d}$ via its Hilbert-Schmidt or Frobenius norm as $\text{Spc}[A] := \|A\|^2/d$ and $\|g\|_{\infty}$ is the absolute largest entry in the gradient vector.

The constant factors f_F and f_g in Theorem 1 are specific to the experimental setup used to estimate the matrix or vector entries. For example, single qubit rotations and two-qubit XX or ZZ gates form ansatz circuits of Pauli rank $r_g = 1$, in which case the factors simplify as $f_F \leq 2$ and $f_g = 1$. The upper bounds in Theorem 1 crucially depend on the regularisation and we prove that $\text{Spc}[\mathbf{F}_Q^{-1}] \leq \eta^{-2}$, refer to Lemma 3 in the Appendix. The explanation is the following. If η is very small then an ill-conditioned inverse might have extreme differences in the magnitude of individual matrix entries – this requires a large number of measurements to sufficiently resolve. Moreover, $\text{Spc}[\mathcal{H}]$ scales with the Pauli rank r_h of the Hamiltonian which typically grows polynomially in the number of qubits. We finally remark that Theorem 1 is quite general and the upper bounds apply to all metric-aware quantum algorithms [31, 32, 35–37] up to minor modifications.

We will establish in the following, that in many cases sampling the gradient vector N_g dominates the overall cost of the natural gradient approach as $N_F + N_g \approx N_g$. Before doing so, let us first bound the sampling cost of the natural gradient vector *relative to* the sampling cost N_{smp} of the gradient vector which could be used directly

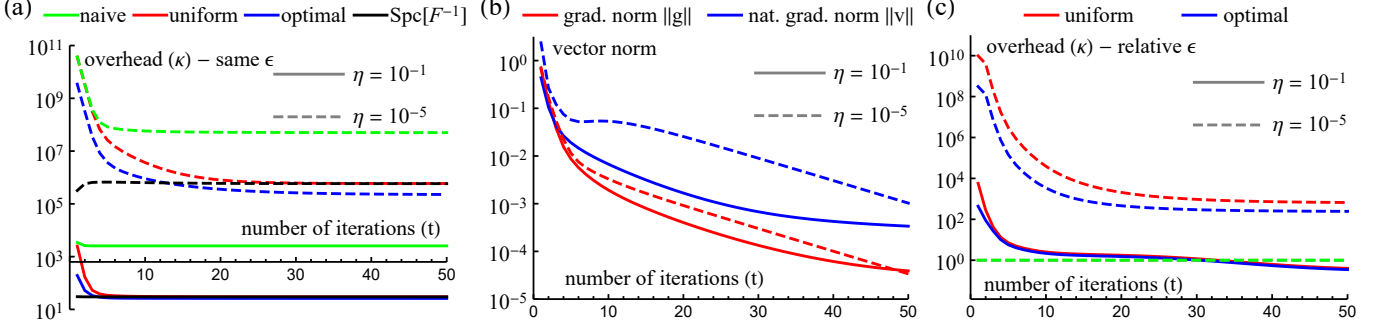


FIG. 1. Exact numerical simulations: a 12-qubit ansatz circuit with 84 parameters is initialised at a good approximation of the ground state of a spin-chain Hamiltonian (refer to Appendix). Natural gradient evolution from Eq. (1) was simulated with a regularisation parameter $\eta = 10^{-1}$ (10^{-5}), see solid (dashed) lines. (a) Measurement overhead κ from Result 1 (red) at every iteration step t of the natural gradient evolution – this quantifies how much more it costs to estimate the natural gradient vector $\underline{v}(t)$ than it would cost to estimate the gradient vector $g(t)$ assuming the same precision ϵ . κ converges to its constant (black) asymptotic approximation determined by the singular values and regularisation of \mathbf{F}_Q . Optimally distributing measurements (blue) via Result 3 significantly reduces sampling costs. However, naively (green) using the same number of measurements for estimating each matrix and vector element results in a substantial overhead. (b) Multiplying $g(t)$ (red) with the inverse of \mathbf{F}_Q results in $\underline{v}(t)$ (blue) whose norm might be orders of magnitude larger. (c) In practice a relative precision is required, such that ϵ is proportional to the vector norms, refer to text. Carefully setting the regularisation parameter η significantly improves the practical applicability: solid lines with $\eta = 10^{-1}$ result in a sampling cost of $\underline{v}(t)$ comparable to (green shows $\kappa = 1$) or even smaller than $g(t)$. Refer to the main text for a remark about mitigating the initial high overheads seen in graphs (a) and (c).

in a simple gradient descent optimisation. We assume the fixed precision $\epsilon^2 = \langle \|\Delta g\|^2 \rangle$.

Theorem 2. *Determining the natural gradient vector to the same precision ϵ as the gradient vector requires a sampling overhead $\kappa := (N_F + N_g)/N_{\text{smp}}.$ This overhead is upper bounded in general*

$$\kappa \leq \eta^{-2} + y, \quad \text{and} \quad \kappa \approx \text{Spc}[\mathbf{F}_Q^{-1}] + y,$$

up to the potentially vanishing term $y = N_F/N_{\text{smp}},$ as in Result 1 and Result 2. Here η is either a regularisation parameter or the smallest singular value of $\mathbf{F}_Q.$ The second equality establishes an approximation as a constant factor which is valid, e.g., when the evolution is close to the optimal point.

Scaling as a function of the iterations — Theorem 1 establishes that the sampling cost N_F of the matrix \mathbf{F}_Q depends on the norm of the gradient vector, which is expected to decrease polynomially during an optimisation – while all other components are constant. In a typical scenario we expect that, even if initially estimating the matrix dominates the sampling costs, asymptotically sampling the vector g dominates the costs. We now state our result which establishes that obtaining the natural gradient vector to the same precision ϵ is only a constant factor more expensive asymptotically than obtaining the gradient vector – where the latter could be used in a simple gradient descent optimisation.

Result 1. *The upper bound in Theorem 1 results in the growth rate $N_F + N_g = \mathcal{O}(\|g(t)\|_\infty^2) + N_g$ when viewed as a function of iterations or steps $t.$ Assuming polynomial convergence via $\|g(t)\|_\infty = \mathcal{O}(t^{-c})$ with $c > 0,$ the*

natural gradient vector requires only a constant sampling overhead asymptotically as

$$\kappa = (N_F + N_g)/N_{\text{smp}} = \mathcal{O}(\text{Spc}[\mathbf{F}_Q^{-1}] + t^{-2c}),$$

when compared to the gradient vector via Theorem 2. We remark that convergence is guaranteed under certain smoothness conditions [26].

We have numerically simulated the natural gradient evolution from Eq. (1) and determined its overhead $\kappa.$ This quantifies how much more it costs at every iteration step t to estimate the natural gradient vector $\underline{v}(t)$ than it would cost to estimate the gradient vector $g(t)$ assuming the same precision $\epsilon.$ Fig 1 (a/red) shows how this sampling overhead converges to its constant asymptotic approximation as the average squared singular values $\text{Spc}[\mathbf{F}_Q^{-1}] \approx 10^6$ ($10^{1.5}$) in Fig 1 (a/black). Fig 1 (a/dashed) also demonstrates that under-regularising the inverse (via $\eta = 10^{-5}$) results in unfeasible sampling costs. In fact, carefully increasing the regularisation parameter (as $\eta = 10^{-1}$) reduces the sampling cost by several orders of magnitude without significantly affecting the performance: both evolutions decrease the gradient norm with a similar rate, compare solid and dashed red lines in Fig 1 (b). Note that the gradient norm does not explicitly depend on the regularisation and its growth rate characterises how fast the optimum is approached.

It is striking that the overhead plotted in Fig 1 (a) can be very high initially; while the focus of the present paper is on the asymptotic costs with respect to time and size, it is worth noting that this high initial cost could be straightforwardly mitigated by, e.g., only occasionally updating a low-rank approximation of the metric tensor.

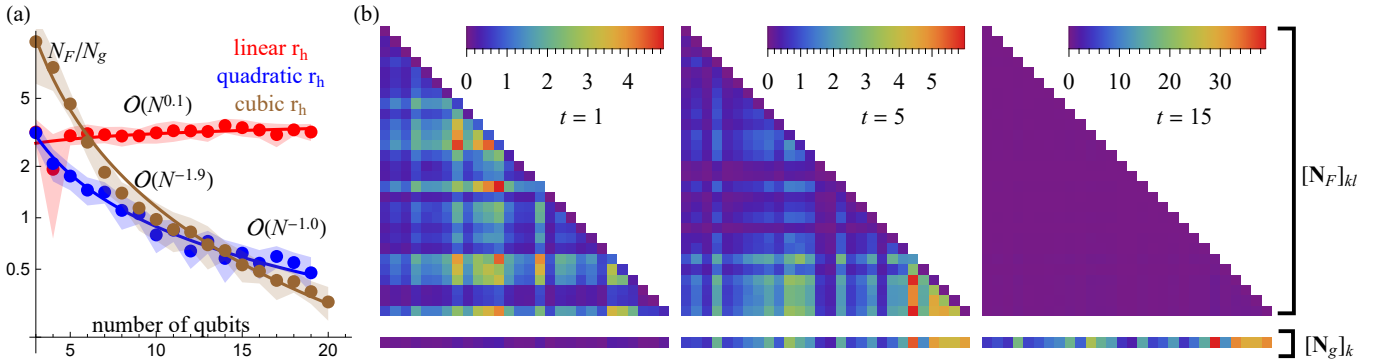


FIG. 2. (a) Sampling cost N_F of the matrix \mathbf{F}_Q relative to the sampling cost N_g of the gradient vector g from Theorem 1 for an increasing number of qubits determined for randomly selected parameters with a fixed $\|g\| = 0.1$. The relative sampling cost N_F/N_g vanishes asymptotically if the number of Pauli terms r_h in the Hamiltonian grows quadratically (blue), cubically (brown) or beyond as established in Eqs. (5-6), refer also to Result 2. In contrast if r_h grows only linearly (red), sampling the matrix \mathbf{F}_Q will dominate the measurement costs for an increasing number of qubits. Shading represents the standard deviation, refer to Appendix. (b) Color-maps showing the optimal number of measurements, $[N_F]_{kl}$ and $[N_g]_k$ assigned to individual elements of the Fisher matrix and gradient respectively after 1, 5, 15 iterations. For clarity here we have scaled the data by a constant factor such that if measurements were distributed uniformly than every matrix and vector element would receive 1 measurement, i.e, we set the total number of measurements N_{opt} to be the number of degrees of freedom. Most of the measurements are assigned to the gradient vector for an increasing number of iterations, as established in Result 1.

This may be expected to have little impact on the convergence rate since in the early phase the advantage of using natural gradient, rather than simple gradient, is typically less pronounced.

Recall that Fig 1 (a) via Result 1 assumes a constant precision ϵ throughout the evolution which is not practical. In fact, one would require a relative precision such that $\epsilon = \epsilon_0 \|g(t)\|$ in case of the gradient vector and $\epsilon = \epsilon_0 \|\underline{v}(t)\|$ in case of the natural gradient vector, for some fixed ϵ_0 . Comparing red and blue lines in Fig 1 (b) illustrates that $\|\underline{v}(t)\|$ can be orders of magnitude larger than $\|g(t)\|$ [42]. We plot the measurement overhead in this relative-precision scheme in Fig 1 (c/red): using a moderate regularisation of the inverse as $\eta = 0.1$, the cost of estimating $\underline{v}(t)$ is comparable or even smaller than estimating $g(t)$, see [Fig 1 (c/red) solid]. Note that we assume a fixed step size λ in Eq. (1) – one could of course determine the optimal magnitude of the step vector $\lambda g(t)$ on-the-fly (although its sampling cost might be comparable to estimating an over-regularised inverse \mathbf{F}_Q^{-1}).

We finally stress that in Fig. 1 we do not actually compare the overall performance of the two optimisation methods – gradient descent would follow significantly different evolution paths resulting in slower convergence. We therefore speculate that, when carefully regularising the metric tensor \mathbf{F}_Q , the natural gradient optimisation might require less sampling overall as it might reach the optimum in significantly fewer iterations [31, 32, 34]. Moreover, we prove in the following that the significant initial overheads on Fig 1 (a-c) do in many practical applications asymptotically vanish for an increasing number of qubits.

Scaling with the system size — Let us now consider how

the upper bounds in Theorem 1 scale with the number of qubits N . First, we consider the general growth rate $\nu = \mathcal{O}(Na(N))$ of the number of parameters ν where $a(N)$ is the depth of the ansatz circuit. For example, polylog(N)-depth circuits constitute a very general class of ansätze via $a(N) = \mathcal{O}(x \log(N)^y)$ for some $x, y > 0$. Second, we establish that the spectral quantity scales with the number of qubits as $\text{Spc}[\mathbf{F}_Q^{-1}] = \mathcal{O}(N^{-s} a^{-s}(N))$ with $0 \leq s \leq 2$, refer to Lemma 3 in the Appendix. Third, the operator norm $\text{Spc}[\mathcal{H}] = \mathcal{O}(r_h) = \mathcal{O}(N^b)$ scales with the Pauli rank of the Hamiltonian r_h which typically grows polynomially with the system size via $b \geq 1$, refer to Appendix. We finally obtain the growth rates

$$N_F = \mathcal{O}(N^{4-2s} a^{4-2s}(N) \|g\|_\infty^2), \quad (5)$$

$$N_g = \mathcal{O}(N^{2-s+b} a^{2-s}(N)). \quad (6)$$

Note that the vector norm $\|g\|_\infty^2$ might in general also depend on the number of qubits. For instance, one can easily construct examples where the norm of the gradient vanishes exponentially as $\|g\|_\infty^2 = \mathcal{O}(\exp(-cN))$ for some $c > 0$, such as in case of barren plateaus [43–45] assuming randomly chosen parameters. In contrast, we now assume that the evolution is initialised in a close vicinity of the optimal parameters (good classical guess is known) and the gradient norm $\|g\|_\infty$ is fixed (bounded). We summarise the resulting measurement cost in the following.

Result 2. *Assume that the number of Pauli terms in the Hamiltonian grows polynomially as $r_h = \mathcal{O}(N^b)$ and the gradient norm $\|g\|_\infty$ is fixed. The relative sampling cost of the matrix \mathbf{F}_Q vanishes for general polylog(N)-depth circuits when $b > (2-s)$ and, following Theorem 2, determining the natural gradient vector requires at most*

a constant overhead asymptotically

$$\kappa = (N_F + N_g)/N_{\text{smp}} = \mathcal{O}(\text{Spc}[\mathbf{F}_Q^{-1}] + N^{2-b}),$$

when compared to the gradient vector.

Note that Result 2 guarantees a vanishing sampling cost of the matrix \mathbf{F}_Q when the number of terms in the Hamiltonian grows faster than quadratically, i.e., $b > 2$, as illustrated in Fig 2. We remark that this result can be applied to the general class of metric-aware quantum algorithms [31, 32, 35–37].

Optimal measurement distribution — So far we have assumed that N_F (N_g) measurements are distributed uniformly among the ν^2 (ν) matrix (vector) entries. However, the overall number of samples $N_F + N_g$ (from Theorem 1), needed to obtain the vector $v = [\mathbf{F}_Q]^{-1} \underline{g}$ to a precision ϵ , can be minimised by distributing samples between the elements of \mathbf{F}_Q and \underline{g} optimally [29]. We denote the matrix $[\mathbf{N}_F]_{kl}$ and the vector $[\mathbf{N}_g]_k$ entries that represent the number of measurements assigned to individual elements in \mathbf{F}_Q and in \underline{g} , respectively. The number of samples required is reduced to $N_{\text{opt}} = \Sigma^2/\epsilon^2$ with $N_{\text{opt}} \leq N_F + N_g$. We now state explicit expressions for determining Σ , $[\mathbf{N}_F]_{kl}$ and $[\mathbf{N}_g]_k$.

Result 3. *Measurements are distributed optimally when the number of samples for determining individual elements of the matrix and gradient are given by*

$$[\mathbf{N}_F]_{kl} = \epsilon^{-2} \Sigma \sqrt{a_{kl} \text{Var}\{[\mathbf{F}_Q]_{kl}\}}, \quad (7)$$

$$[\mathbf{N}_g]_k = \epsilon^{-2} \Sigma \sqrt{b_k \text{Var}[g_k]}, \quad (8)$$

respectively. Here $\text{Var}[\cdot]$ is the variance of a single measurement of the corresponding element and we explicitly define Σ via the coefficients a_{kl} and b_k as

$$\Sigma := \sum_{k,l=1}^{\nu} \sqrt{a_{kl} \text{Var}\{[\mathbf{F}_Q]_{kl}\}} + \sum_{k=1}^{\nu} \sqrt{b_k \text{Var}[g_k]}. \quad (9)$$

Furthermore, the symmetry of the Fisher matrix can be explicitly included just by modifying the coefficients a_{kl} , as discussed in the Appendix.

We remark that this result is completely general and can be applied to any of the metric-aware quantum algorithms [31, 32, 35–37].

[Fig. 1 (a/c) blue] shows how the optimal distribution of samples reduces the measurement overhead across the entire evolution – most significantly for small regularisation parameters [Fig. 1 (a/c), $\eta = 10^{-5}$], in which case some matrix elements might be crucially larger than others. Moreover, result 3 automatically takes into account the decreasing sampling cost of the matrix as established in Results 1-2. This is illustrated in Fig 2 (b); For the first few iterations, far from convergence, the bulk of the measurements are directed to the matrix, comparatively few go to the elements of the gradient [Fig 2 (b), $t = 1$]. However, close to convergence, consistent with Result 1,

the gradient takes the majority of the measurements, [Fig 2 (b), $t = 20$].

Discussion and conclusion — In this work we established general upper bounds on the sampling cost of noise-aware variational quantum algorithms. We analysed how this sampling cost scales for increasing iterations in Result 1 and for increasing qubit numbers in Result 2. The latter establishes that the relative measurement cost of the matrix object \mathbf{F}_Q is asymptotically negligible in many practically relevant scenarios, such as in case of quantum chemistry applications.

Natural gradient has been shown to outperform other optimisation approaches in numerical simulations [31, 32, 34]. We proved in this work that for both an increasing number of iterations and number of qubits the sampling overhead of the natural gradient approach is constant asymptotically. We therefore speculate, that this technique might reach the optimum in fewer overall samples than simple gradient descent. Furthermore, this constant overhead strongly depends on the regularisation parameter η that is used in the classical step of matrix inversion. We conclude that η needs to be carefully set in practice: it allows to significantly reduce sampling costs of metric-aware algorithms without affecting their performance.

We finally established a general technique that optimally distributes measurements when estimating matrix and vector entries, further reducing the cost of general metric-aware quantum algorithms. Despite the favourable asymptotic scaling of natural gradient, a significant overhead might be expected for low-qubit applications at the first few iteration steps. In future work we aim to develop approaches which mitigate this overhead by only occasionally updating an approximation of the metric tensor.

ACKNOWLEDGMENTS

B. K. acknowledges funding received from EU H2020-FETFLAG-03-2018 under the grant agreement No 820495 (AQTION). The authors thank Simon C. Benjamin and Natalia Ares for their support, stimulating ideas and useful comments on this manuscript. Numerical simulations in this work used the QuEST and QuESTlink quantum simulation packages [46, 47]. The authors would like to acknowledge the use of the University of Oxford Advanced Research Computing (ARC) facility in carrying out this work. We thank Patrick Coles and Andrew Arrasmith for their useful comments.

[1] Edward Farhi, Jeffrey Goldstone, and Sam Gutmann. A quantum approximate optimization algorithm. *arXiv preprint arXiv:1411.4028*, 2014.

[2] Alberto Peruzzo, Jarrod McClean, Peter Shadbolt, Man-Hong Yung, Qi Zhou, Peter J Love, Alán Aspuru-Guzik, and Jeremy L O’Brien. A variational eigenvalue solver on a photonic quantum processor. *Nature communications*, 5, 2014.

[3] Ya Wang, Florian Dolde, Jacob Biamonte, Ryan Babbush, Ville Bergholm, Sen Yang, Ingmar Jakobi, Philipp Neumann, Alán Aspuru-Guzik, James D Whitfield, et al. Quantum simulation of helium hydride cation in a solid-state spin register. *ACS nano*, 9(8):7769–7774, 2015.

[4] P. J. J. O’Malley, R. Babbush, I. D. Kivlichan, J. Romero, J. R. McClean, R. Barends, J. Kelly, P. Roushan, A. Tranter, N. Ding, B. Campbell, Y. Chen, Z. Chen, B. Chiaro, A. Dunsworth, A. G. Fowler, E. Jeffrey, E. Lucero, A. Megrant, J. Y. Mutus, M. Neeley, C. Neill, C. Quintana, D. Sank, A. Vainsencher, J. Wenner, T. C. White, P. V. Coveney, P. J. Love, H. Neven, A. Aspuru-Guzik, and J. M. Martinis. Scalable Quantum Simulation of Molecular Energies. *Phys. Rev. X*, 6:031007, Jul 2016.

[5] Yangchao Shen, Xiang Zhang, Shuaining Zhang, Jing-Ning Zhang, Man-Hong Yung, and Kihwan Kim. Quantum implementation of the unitary coupled cluster for simulating molecular electronic structure. *Phys. Rev. A*, 95:020501, Feb 2017.

[6] Jarrod R McClean, Jonathan Romero, Ryan Babbush, and Alán Aspuru-Guzik. The theory of variational hybrid quantum-classical algorithms. *New J. Phys.*, 18(2):023023, 2016.

[7] S. Paesani, A. A. Gentile, R. Santagati, J. Wang, N. Wiebe, D. P. Tew, J. L. O’Brien, and M. G. Thompson. Experimental Bayesian Quantum Phase Estimation on a Silicon Photonic Chip. *Phys. Rev. Lett.*, 118:100503, Mar 2017.

[8] Ying Li and Simon C. Benjamin. Efficient Variational Quantum Simulator Incorporating Active Error Minimization. *Phys. Rev. X*, 7:021050, Jun 2017.

[9] J. I. Colless, V. V. Ramasesh, D. Dahlen, M. S. Blok, M. E. Kimchi-Schwartz, J. R. McClean, J. Carter, W. A. de Jong, and I. Siddiqi. Computation of Molecular Spectra on a Quantum Processor with an Error-Resilient Algorithm. *Phys. Rev. X*, 8:011021, Feb 2018.

[10] Raffaele Santagati, Jianwei Wang, Antonio A. Gentile, Stefano Paesani, Nathan Wiebe, Jarrod R. McClean, Sam Morley-Short, Peter J. Shadbolt, Damien Bonneau, Joshua W. Silverstone, David P. Tew, Xiaoqi Zhou, Jeremy L. O’Brien, and Mark G. Thompson. Witnessing eigenstates for quantum simulation of Hamiltonian spectra. *Science Advances*, 4(1), 2018.

[11] Abhinav Kandala, Antonio Mezzacapo, Kristan Temme, Maika Takita, Markus Brink, Jerry M Chow, and Jay M Gambetta. Hardware-efficient variational quantum eigensolver for small molecules and quantum magnets. *Nature*, 549(7671):242, 2017.

[12] Abhinav Kandala, Kristan Temme, Antonio D Córcoles, Antonio Mezzacapo, Jerry M Chow, and Jay M Gambetta. Error mitigation extends the computational reach of a noisy quantum processor. *Nature*, 567(7749):491, 2019.

[13] Cornelius Hempel, Christine Maier, Jonathan Romero, Jarrod McClean, Thomas Monz, Heng Shen, Petar Jurcevic, Ben P. Lanyon, Peter Love, Ryan Babbush, Alán Aspuru-Guzik, Rainer Blatt, and Christian F. Roos. Quantum Chemistry Calculations on a Trapped-Ion Quantum Simulator. *Phys. Rev. X*, 8:031022, Jul 2018.

[14] Jonathan Romero, Ryan Babbush, Jarrod R McClean, Cornelius Hempel, Peter Love, and Alán Aspuru-Guzik. Strategies for quantum computing molecular energies using the unitary coupled cluster ansatz. *arXiv preprint arXiv:1701.02691*, 2017.

[15] Oscar Higgott, Daochen Wang, and Stephen Brierley. Variational Quantum Computation of Excited States. *arXiv preprint arXiv:1805.08138*, 2018.

[16] Jarrod R McClean, Mollie E Kimchi-Schwartz, Jonathan Carter, and Wibe A de Jong. Hybrid quantum-classical hierarchy for mitigation of decoherence and determination of excited states. *Physical Review A*, 95(4):042308, 2017.

[17] James I Colless, Vinay V Ramasesh, Dar Dahlen, Machiel S Blok, Jarrod R McClean, Jonathan Carter, Wibe A de Jong, and Irfan Siddiqi. Robust determination of molecular spectra on a quantum processor. *arXiv preprint arXiv:1707.06408*, 2017.

[18] Christian Kokail, Christine Maier, Rick van Bijnen, Tiff Brydges, Manoj K Joshi, Petar Jurcevic, Christine A Muschik, Pietro Silvi, Rainer Blatt, Christian F Roos, et al. Self-Verifying Variational Quantum Simulation of the Lattice Schwinger Model. *arXiv preprint arXiv:1810.03421*, 2018.

[19] Kunal Sharma, Sumeet Khatri, Marco Cerezo, and Patrick J Coles. Noise resilience of variational quantum compiling. *New Journal of Physics*, 22(4):043006, 2020.

[20] M Cerezo, Kunal Sharma, Andrew Arrasmith, and Patrick J Coles. Variational Quantum State Eigensolver. *arXiv preprint arXiv:2004.01372*, 2020.

[21] John Preskill. Quantum Computing in the NISQ era and beyond. *arXiv preprint arXiv:1801.00862*, 2018.

[22] Ivan Kassal, James D Whitfield, Alejandro Perdomo-Ortiz, Man-Hong Yung, and Alán Aspuru-Guzik. Simulating chemistry using quantum computers. *Annual review of physical chemistry*, 62:185–207, 2011.

[23] Dawei Lu, Boruo Xu, Nanyang Xu, Zhaokai Li, Hongwei Chen, Xinhua Peng, Ruixue Xu, and Jiangfeng Du. Quantum chemistry simulation on quantum computers: theories and experiments. *Phys. Chem. Chem. Phys.*, 14:9411–9420, 2012.

[24] K Birgitta Whaley, Aaron R Dinner, and Stuart A Rice. *Quantum information and computation for chemistry*. John Wiley & Sons, 2014.

[25] Sam McArdle, Suguru Endo, Alan Aspuru-Guzik, Simon Benjamin, and Xiao Yuan. Quantum computational chemistry. *arXiv preprint arXiv:1808.10402*, 2018.

[26] Ryan Sweke, Frederik Wilde, Johannes Meyer, Maria Schuld, Paul K Fährmann, Barthélémy Meynard-Piganeau, and Jens Eisert. Stochastic gradient descent for hybrid quantum-classical optimization. *arXiv preprint arXiv:1910.01155*, 2019.

[27] Jonas M Kübler, Andrew Arrasmith, Lukasz Cincio, and Patrick J Coles. An adaptive optimizer for measurement-frugal variational algorithms. *arXiv preprint arXiv:1909.09083*, 2019.

[28] Laura Gentini, Alessandro Cuccoli, Stefano Pirandola, Paola Verrucchi, and Leonardo Banchi. Noise-Assisted Variational Hybrid Quantum-Classical Optimization. *arXiv preprint arXiv:1912.06744*, 2019.

[29] Ophelia Crawford, Barnaby van Straaten, Daochen Wang, Thomas Parks, Earl Campbell, and Stephen Brierley. Efficient quantum measurement of Pauli operators. pages 1–15, 2019.

[30] Andrew Arrasmith, Lukasz Cincio, Rolando D Somma, and Patrick J Coles. Operator Sampling for Shot-frugal Optimization in Variational Algorithms. *arXiv preprint arXiv:2004.06252*, 2020.

[31] Bálint Koczor and Simon C Benjamin. Quantum natural gradient generalised to non-unitary circuits. *arXiv preprint arXiv:1912.08660*, 2019.

[32] Sam McArdle, Tyson Jones, Suguru Endo, Ying Li, Simon C Benjamin, and Xiao Yuan. Variational ansatz-based quantum simulation of imaginary time evolution. *npj Quantum Information*, 5(1):1–6, 2019.

[33] Patrick Rebentrost, Maria Schuld, Leonard Wossnig, Francesco Petruccione, and Seth Lloyd. Quantum gradient descent and Newton’s method for constrained polynomial optimization. *New Journal of Physics*, 21(7):073023, jul 2019.

[34] David Wierichs, Christian Gogolin, and Michael Kastoryano. Avoiding local minima in variational quantum eigensolvers with the natural gradient optimizer. *arXiv preprint arXiv:2004.14666*, 2020.

[35] Ying Li and Simon C Benjamin. Efficient variational quantum simulator incorporating active error minimization. *Phys. Rev. X*, 7(2):021050, 2017.

[36] Xiao Yuan, Suguru Endo, Qi Zhao, Ying Li, and Simon C Benjamin. Theory of variational quantum simulation. *Quantum*, 3:191, 2019.

[37] James Stokes, Josh Izaac, Nathan Killoran, and Giuseppe Carleo. Quantum natural gradient. *arXiv preprint arXiv:1909.02108*, 2019.

[38] Where the ansatz parameter θ corresponds to a global Z rotation of all the qubits and therefore $r_g = N$. Here N is the number of qubits.

[39] Luca Pezzè, Augusto Smerzi, Markus K. Oberthaler, Roman Schmied, and Philipp Treutlein. Quantum metrology with nonclassical states of atomic ensembles. *Rev. Mod. Phys.*, 90:035005, Sep 2018.

[40] Vittorio Giovannetti, Seth Lloyd, and Lorenzo Maccone. Advances in quantum metrology. *Nat. Phot.*, 5(4):222, 2011.

[41] Bálint Koczor, Suguru Endo, Tyson Jones, Yuichiro Matsuzaki, and Simon C Benjamin. Variational-State Quantum Metrology. *arXiv preprint arXiv:1908.08904*, 2019.

[42] As the number of iterations increases, the gradient vector has an increasing overlap with the subspace that corresponds to small singular values of the QFI matrix – and it follows that this contribution in the gradient vector is non-trivially magnified by the inverse matrix.

[43] Jarrod R McClean, Sergio Boixo, Vadim N Smelyanskiy, Ryan Babbush, and Hartmut Neven. Barren plateaus in quantum neural network training landscapes. *Nature communications*, 9(1):1–6, 2018.

[44] Edward Grant, Leonard Wossnig, Mateusz Ostaszewski, and Marcello Benedetti. An initialization strategy for addressing barren plateaus in parametrized quantum circuits. *Quantum*, 3:214, 2019.

[45] M Cerezo, Akira Sone, Tyler Volkoff, Lukasz Cincio, and Patrick J Coles. Cost-Function-Dependent Barren Plateaus in Shallow Quantum Neural Networks. *arXiv preprint arXiv:2001.00550*, 2020.

[46] Tyson Jones, Anna Brown, Ian Bush, and Simon C Benjamin. QuEST and high performance simulation of quantum computers. *Sci. Rep.*, 9(1):10736, 2019.

[47] Tyson Jones and Simon C Benjamin. QuESTlink–Mathematica embiggened by a hardware-optimised quantum emulator. *Quantum Science and Technology*, 2020.

[48] H.H. Ku. Notes on the use of propagation of error formulas. *Journal of Research of the National Bureau of Standards, Section C: Engineering and Instrumentation*, 70C(4):263, 1966.

[49] M. Lefebvre, R. K. Keeler, R. Sobie, and J. White. Propagation of errors for matrix inversion. *Nuclear Instruments and Methods in Physics Research, Section A: Accelerators, Spectrometers, Detectors and Associated Equipment*, 451(2):520–528, 2000.

Appendix A: Determining variances

1. Pauli decompositions

Let us denote the set of Hermitian matrices of dimension d as $\text{Herm}[\mathbb{C}^{d \times d}]$. The Hamiltonian $\mathcal{H} \in \text{Herm}[\mathbb{C}^{d \times d}]$ of a qubit-system in general decomposes into a sum over Pauli-operator strings via

$$\mathcal{H} = \sum_{l=1}^{r_h} h_l P_l, \quad \text{with} \quad \mathbb{R} \ni h_l := \text{Tr}[\mathcal{H} P_l]/d, \quad (\text{A1})$$

where $P_l \in \text{Herm}[\mathbb{C}^{d \times d}]$ are tensor products of single-qubit Pauli operators that act on an N -qubit system and form an orthonormal basis of the Hilbert-Schmidt operator space, and $d = 2^N$ is the dimensionality. We denote as $r_h \in \mathbb{N}$ the Pauli rank, i.e., the number of non-zero Pauli components in the Hamiltonian. Note that in general $r_h \leq 4^N$.

In the following derivations we assume for simplicity that ansatz circuits U_c are unitary and decomposes into a product of individual gates

$$U_c(\underline{\theta}) = U_\nu(\theta_\nu) \dots U_2(\theta_2) U_1(\theta_1), \quad (\text{A2})$$

that typically act on a small subset of the system, e.g., one and two-qubit gates. We assume in Eq. (A2) for ease of notation that each quantum gate depends on an individual parameter θ_i with $i = \{1, 2, \dots, \nu\}$.

Individual gates $U_k(\theta_k) \in SU(d)$ of the quantum circuit from Eq. (A2) are in general of the form $U_k(\theta_k) := \exp[-i\theta_k G_k]$ and their generators $G_k \in \text{Herm}[\mathbb{C}^{d \times d}]$ decompose into a sum of Pauli strings resulting in

$$U_k(\theta_k) = \exp[-i\theta_k G_k] = \exp[-i\theta_k \sum_{l=1}^{r_g^{(k)}} g_{kl} P_l], \quad \text{with} \quad \mathbb{R} \ni g_{kl} := \text{Tr}[G_k P_l]/d$$

and $r_g^{(k)} \in \mathbb{N}$ is the Pauli rank of the generator G_k . We additionally assume that $g_{kl} \leq 1/2$ for simplicity – but any other upper bound could be specified. It follows in general that the derivative $\partial_k U_k(\theta_k)$ decomposes into a sum of $r_g^{(k)}$ unitary operators as

$$\partial_k U_k(\theta_k) = -i \sum_{l=1}^{r_g^{(k)}} g_{kl} P_l U_k(\theta_k). \quad (\text{A3})$$

For ease of notation, in the following we consider circuits via Eq. (A2) which decompose into gates $U_k(\theta_k)$ with Pauli rank $r_g = 1$. This is naturally the case for a wide variety of ansatz circuits, e.g., circuits that consist of single-qubit rotations and two-qubit ZZ or XX evolution gates as depicted in Fig. 3. This assumption results in a simplified structure of the gates as $U_k(\theta_k) := \exp[-i\theta_k P_k/2]$ and their derivatives as

$$\partial_k U_k(\theta_k) = -\frac{i}{2} P_k U_k(\theta_k), \quad (\text{A4})$$

where P_k is the Pauli generator of the gate $U_k(\theta_k)$. This construction simplifies our following derivations, however, the generalisation to arbitrary parametrised gates straightforwardly follows from linearity of Eq. (A3).

We finally define the partial derivative of the circuit in Eq. (A2) using our simplified ansatz as

$$D_k := 2i \partial_k U_c(\underline{\theta}) = U_\nu(\theta_\nu) \dots P_k U_k(\theta_k) \dots U_2(\theta_2) U_1(\theta_1),$$

which itself is unitary via $[D_k]^\dagger = [D_k]^{-1}$ (and we omit its explicit dependence on the parameters $\underline{\theta}$) and $P_l P_l^\dagger = \text{Id}_d$.

We remark that in case of non-unitary parametrisations one would need to consider the general mapping $\rho(\underline{\theta}) := \Phi(\underline{\theta}) \rho_0$. The circuit derivative then decomposes into Pauli terms as

$$\partial_k \rho(\underline{\theta}) = \sum_{m,n=1}^{r_p^{(k)}} p_{kmn} P_m \rho(\underline{\theta}) P_n. \quad (\text{A5})$$

2. Upper bound on the quantum Fisher information

We now derive a general upper bound on the quantum Fisher information for unitary parametrisations.

Lemma 1. *In case of unitary ansatz circuits that act on arbitrary quantum states ρ via quantum gates that decompose into at most r_g Pauli terms, entries of the quantum Fisher information matrix are upper bounded as $[\mathbf{F}_Q]_{kl} \leq r_g^2$.*

Proof. When the ansatz circuit consists of unitary gates, the quantum Fisher information assumes its maximum for pure states. Considering the pure state $\rho = |\psi\rangle\langle\psi|$, it follows from [31] that

$$[\mathbf{F}_Q]_{kl} = 2 \operatorname{Tr}[(\partial_k \rho)(\partial_l \rho)].$$

Applying the CauchySchwarz inequality yields

$$2\operatorname{Tr}[(\partial_k \rho)(\partial_l \rho)] \leq 2\sqrt{\operatorname{Tr}[(\partial_k \rho)(\partial_k \rho)] \operatorname{Tr}[(\partial_l \rho)(\partial_l \rho)]} \leq F_{max}$$

where F_{max} is a bound on the scalar quantum Fisher information, i.e., diagonal entries of the matrix \mathbf{F}_Q . Let us determine this bound via

$$[\mathbf{F}_Q]_{kk} = 4\operatorname{Re}[\langle \partial_k \psi | \partial_k \psi \rangle] - 4|\langle \partial_k \psi | \psi \rangle|^2 \leq 4\operatorname{Re}[\langle \partial_k \psi | \partial_k \psi \rangle] = 4\langle \partial_k \psi | \partial_k \psi \rangle \quad (\text{A6})$$

for an arbitrary $|\psi\rangle$. It follows from Eq. (A3) that

$$\langle \partial_k \psi | \partial_k \psi \rangle = \sum_{l,m=1}^{r_g^{(k)}} g_{kl} g_{km} \langle \psi_l | \psi_m \rangle \leq (r_g)^2 / 4, \quad (\text{A7})$$

where $|\psi_m\rangle$ are some valid, normalised states and therefore $\langle \psi_l | \psi_m \rangle \leq 1$ and we used that $g_{kl} \leq 1/2$. This finally establishes the general upper bound for unitary ansatz circuits whose gates decompose into at most r_g Pauli terms as

$$[\mathbf{F}_Q]_{kl} \leq r_g^2$$

and in case of simplified ansätze with $r_g = 1$ from Sec. A 1 one obtains $[\mathbf{F}_Q]_{kl} \leq 1$. □

3. Components of the gradient

Components of the gradient vector can be measured via Hadamard test. We discuss this on the example of simplified ansätze from Sec. A 1, while the generalisation follows from linearity. Let us first express the gradient components $g_k := \partial_k E(\underline{\theta})$ in terms of the derivative circuits from Eq. A4 as

$$g_k = -\operatorname{Im}[\langle 0 | [D_k]^\dagger \mathcal{H} U_c | 0 \rangle] = -\sum_{l=1}^{r_h} h_l M_{kl},$$

where the second equation uses the decomposition of the Hamiltonian into Pauli operators from Eq. (A1) via denoting the matrix elements $M_{kl} := \operatorname{Im}\langle 0 | [D_k]^\dagger P_l U_c | 0 \rangle$. These matrix elements can be estimated by using an ancilla qubit via the circuits in Fig. 2 of reference [8] and the corresponding proof can be found in footnote [53] of [8], refer also to [36]. The probability p of measuring this ancilla qubit in the $|\pm\rangle$ basis with outcome $+1$ determines the matrix elements via $(2p_{kl} - 1) = M_{kl}$ for every Pauli component in the Hamiltonian P_l . This finally yields the explicit form of the gradient vector

$$g_k = \partial_k E(\underline{\theta}) = -\sum_{l=1}^{r_h} h_l (2p_{kl} - 1) \quad (\text{A8})$$

in terms of the measurement probabilities $0 \leq p_{kl} \leq 1$. Note that each probability p_{kl} is estimated by sampling a binomial distribution which has a variance $\sigma_{kl}^2 = p_{kl}(1 - p_{kl})$. It follows that the variance of the gradient components are determined by these individual variances via

$$\operatorname{Var}[g_k] = 4 \sum_{l=1}^{r_h} h_l^2 \sigma_{kl}^2 = 4 \sum_{l=1}^{r_h} h_l^2 p_{kl}(1 - p_{kl}). \quad (\text{A9})$$

Re-expressing this variance in terms of the matrix elements via $p_{kl} = (M_{kl}+1)/2$ yields the simplified form

$$\text{Var}[g_k] = \sum_{l=1}^{r_h} h_l^2 (1 - [M_{kl}]^2). \quad (\text{A10})$$

This expression is related directly to the parametrised quantum state $|\psi(\underline{\theta})\rangle$ via the expectation value as $M_{kl} = -2\text{Re}\langle\partial_k\psi(\underline{\theta})|P_l|\psi(\underline{\theta})\rangle$.

In complete generality, i.e., when gates decompose into a linear combination of at most r_g Pauli terms, the variance of the gradient entries is upper bounded (via Eq. (A9)) as

$$\text{Var}[g_k] \leq r_g \sum_{l=1}^{r_h} h_l^2 = r_g \text{Spc}[\mathcal{H}] = \mathcal{O}(r_g r_h), \quad (\text{A11})$$

where $\text{Spc}[\mathcal{H}]$ follows from the Hilbert-Schmidt scalar product as

$$\text{Spc}[\mathcal{H}] := \|\mathcal{H}\|^2/d := \text{Tr}[\mathcal{H}\mathcal{H}]/d = \sum_{k,l=1}^{r_h} h_k h_l \text{Tr}[P_k P_l]/d = \sum_{l=1}^{r_h} h_l^2 = \mathcal{O}(r_h).$$

via Eq. (A1) and recall that $\text{Tr}[P_k P_l] = d \delta_{kl}$, where δ_{kl} is the Kroenecker delta and $d = 2^N$.

Let us now consider mixed quantum states, e.g., due to gate imperfections, via the eigendecomposition $\rho = \sum_n p_n |\psi_n\rangle\langle\psi_n|$. If the parametrisation $\underline{\theta}$ is approximately unitary via $\frac{\partial p_n}{\partial \theta_k} \approx 0$, then gradient components of the expectation value $\text{Tr}[\rho(\underline{\theta})\mathcal{H}]$ can be expressed as

$$\frac{\partial}{\partial \theta_k} \text{Tr}[\rho(\underline{\theta})\mathcal{H}] \approx \sum_n p_n \frac{\partial}{\partial \theta_k} [\langle\psi_n(\underline{\theta})|\mathcal{H}|\psi_n(\underline{\theta})\rangle] = \sum_n p_n [g_k]_n \quad (\text{A12})$$

where $[g_k]_n$ is the gradient that would be measured by the above protocol for the pure eigenstate $|\psi_n(\underline{\theta})\rangle$. The above discussed protocol therefore estimates the correct gradient for mixed states – as long as the parametrisation is approximately unitary, such as in case of noisy gates. The same upper bound holds for the variances via $\sum_n p_n = 1$ and $0 \leq p_n \leq 1$, and the bound is only saturated by pure states.

In summary, the variance of the gradient entries is upper bounded as $\text{Var}[g_k] \leq \text{Spc}[\mathcal{H}] f_g$, where f_g is a constant factor that only depends on the ansatz structure and on the particular quantum algorithm, e.g., $f_g = r_g$ in case of the natural gradient approach. We remark that the above discussed protocol is used in other metric-aware quantum algorithms and our bounds therefore apply to other vector objects used in these algorithms [31, 32, 35–37].

4. Components of the quantum Fisher information matrix

We will now focus on determining variances of the quantum Fisher information entries $[\mathbf{F}_Q]_{kl}$. For pure states as $\rho = |\psi\rangle\langle\psi|$, entries of the quantum Fisher information can be expressed via the state-vector scalar products [31]

$$[\mathbf{F}_Q]_{kl} = 4\text{Re}[\langle\partial_k\psi|\partial_l\psi\rangle - \langle\partial_k\psi|\psi\rangle\langle\psi|\partial_l\psi\rangle], \quad (\text{A13})$$

The second term in the above equation vanishes when the global phase evolution of $|\psi\rangle$ is zero [36] and an experimental protocol for measuring the remaining component $\text{Re}\langle\partial_k\psi|\partial_l\psi\rangle$ was used in [32] for simulating imaginary time evolution.

We now propose a protocol that determines both terms in Eq. A13. Assuming the simplified ansatz from Sec. A 1, our protocol allows to evaluate the coefficients by measuring an ancilla qubit

$$\begin{aligned} A_{kl} &= 4\text{Re}\langle\partial_k\psi|\partial_l\psi\rangle = \text{Re}\langle 0|[D_k]^\dagger D_l | 0 \rangle = 2[p_a]_{kl} - 1, \\ B_k &= 2\text{Re}\langle\partial_k\psi|\psi\rangle = \text{Re}\langle 0|[D_k]^\dagger U_c | 0 \rangle = 2[p_b]_k - 1, \\ C_k &= 2\text{Im}\langle\partial_k\psi|\psi\rangle = \text{Im}\langle 0|[D_k]^\dagger U_c | 0 \rangle = 2[p_c]_k - 1, \end{aligned}$$

using the circuits in Fig. 2 of reference [8], refer to footnote [53] of [8] for a proof. These circuits allow for estimating the probabilities p_a , p_b and p_c by sampling the ancilla qubit as a binomial distribution. The quantum Fisher information is then obtained as

$$[\mathbf{F}_Q]_{kl} = A_{kl} + B_k B_l - C_k C_l = (2[p_a]_{kl} - 1) + (2[p_b]_k - 1)(2[p_b]_l - 1) - (2[p_c]_k - 1)(2[p_c]_l - 1).$$

Since the probabilities p_a , p_b and p_c are determined from binomial distributions, their variances are given by, e.g., $[\sigma_a^2]_{kl} = [p_a]_{kl}(1 - [p_a]_{kl})$. It follows that

$$\text{Var}\{[\mathbf{F}_Q]_{kl}\} = 4[\sigma_a^2]_{kl} + 4[\sigma_b^2]_k B_l^2 + 4[\sigma_b^2]_l B_k^2 + 4[\sigma_c^2]_k C_l^2 + 4[\sigma_c^2]_l C_k^2,$$

Substituting $4[\sigma_b^2]_k = (1 - [B_l]^2)$ and $4[\sigma_c^2]_k = (1 - [C_l]^2)$, we can express the variances as

$$\text{Var}\{[\mathbf{F}_Q]_{kl}\} = (1 - [A_{kl}]^2) + (1 - [B_k]^2)B_l^2 + (1 - [B_l]^2)B_k^2 + (1 - [C_k]^2)C_l^2 + (1 - [C_l]^2)C_k^2,$$

in terms of the estimated quantities A_{kl} , B_k and C_k , and we used the expressions, e.g., $(A_{kl} + 1)/2 = [p_a]_{kl}$.

Note that the inequality $(1 - [B_k]^2)B_l^2 \leq 1/4$ is saturated when $B_k = 1/\sqrt{2}$ and in general $|A_{kl}|, |B_l|, |C_l| \leq 1$. Using this inequality we can establish the general upper bound

$$\text{Var}\{[\mathbf{F}_Q]_{kl}\} \leq 2r_g^2, \quad (\text{A14})$$

when gates decompose into a linear combination of at most r_g Pauli terms.

When assuming noisy unitary circuits, Result 3 in [31] establishes that $[\mathbf{F}_Q]_{kl} \approx 2\text{Tr}[(\partial_k\rho)(\partial_l\rho)]$ and the approximation becomes exact for pure states as $\rho = |\psi\rangle\langle\psi|$. The Hilbert-Schmidt scalar products $\text{Tr}[(\partial_k\rho)(\partial_l\rho)]$ can be measured using the circuit based on SWAP tests from [36] and one can directly estimate the quantity $[\mathbf{F}_Q]_{kl} = (2p_{kl} - 1)$ by measuring the probability p_{kl} of an ancilla qubit in case when using the simplified ansatz from Sec. A 1, i.e., when gates decompose into single Pauli terms. We remark that this implementation requires more qubits when compared to the above introduced pure-state approach. However, it is preferable as it results in negligible approximation errors when gates are imperfect, refer to [31]. The variance follows as $\text{Var}\{[\mathbf{F}_Q]_{kl}\} = 4p_{kl}(1 - p_{kl}) = (1 - [\mathbf{F}_Q]_{kl}^2) \leq 1$ in case of the simplified ansatz from Sec. A 1 and we have used $[\mathbf{F}_Q]_{kl} \leq 1$ from Lemma 1.

In complete generality, i.e., when gates decompose into a linear combination of at most r_g Pauli terms, the variance of the matrix entries is upper bounded as

$$\text{Var}\{[\mathbf{F}_Q]_{kl}\} \leq r_g^2. \quad (\text{A15})$$

In summary, the variance of the matrix entries are upper bounded as $\text{Var}\{[\mathbf{F}_Q]_{kl}\} \leq f_F$, where f_F is a constant factor that only depends on the ansatz structure and the approach used to estimate the matrix entries. We remark that the above discussed two protocols are used in other metric-aware quantum algorithms and our bounds therefore apply to other matrix objects estimated by these algorithms [31, 32, 35–37].

5. Numerical simulations

In our numerical simulations we use the ansatz illustrated in Fig. 3. This decomposes into repeated blocks. The first block B_1 consists of single-qubit X rotations while the second block B_2 decomposes into nearest-neighbour Pauli ZZ gates followed by single qubit Y and X rotations. Each gate depends on an individual parameter θ_k with $k \in \{1 \dots \nu\}$. In our numerical simulations we use the ansatz structure $B_1 B_2 B_2$ which has a linearly growing number of parameters $\nu = \mathcal{O}(N)$ in the number of qubits via the constant depth $a(N) = \mathcal{O}(N^0)$.

In Fig. 1 we simulate the natural gradient approach for finding the ground state energy of the spin-chain Hamiltonian

$$\mathcal{H} = \sum_{i=1}^{N-1} J[\sigma_x^{(i)}\sigma_x^{(i+1)} + \sigma_y^{(i)}\sigma_y^{(i+1)} + \sigma_z^{(i)}\sigma_z^{(i+1)}] + J[\sigma_x^{(1)}\sigma_x^{(N)} + \sigma_y^{(1)}\sigma_y^{(N)} + \sigma_z^{(1)}\sigma_z^{(N)}] + \sum_{i=1}^N \omega_i \sigma_z^{(i)}. \quad (\text{A16})$$

which contains identical couplings xx , yy and zz between nearest neighbours with a constant which we set $J = 1$. Here $\sigma_\alpha^{(k)}$ represent Pauli matrices acting on qubit k with $\alpha = \{x, y, z\}$. We select on-site frequencies ω_i randomly according to a uniform distribution with values varying between -1 and 1 . The resulting Hamiltonian has a non-trivial, highly entangled ground state that we aim to approximate using the (not necessarily optimal) ansatz circuit shown on Fig. 3. We initialise the optimisation at a point in parameter space close to the optimum and we set the step size as $\lambda = 0.2$.

In Fig. 2 we simulate various different Hamiltonians using the same technique. In particular, we use Eq. (A16) as the linearly scaling Hamiltonian in Fig. 2 (red). We define the quadratically scaling Hamiltonian Fig. 2 (blue) as

$$\mathcal{H} = \sum_{k>l=1}^N J[\sigma_x^{(k)}\sigma_x^{(l)} + \sigma_y^{(k)}\sigma_y^{(l)} + \sigma_z^{(k)}\sigma_z^{(l)}] + \sum_{k=1}^N \omega_k \sigma_z^{(k)}, \quad (\text{A17})$$

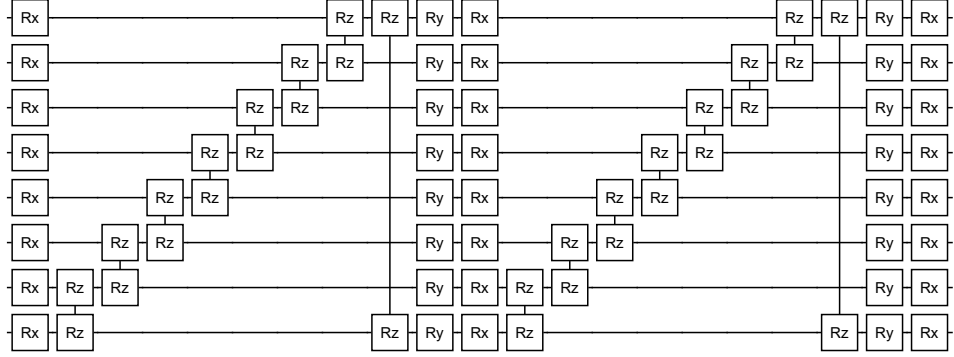


FIG. 3. Example of an 8-qubit ansatz structure used in our simulations. It consists of repeated blocks of single qubit X and Y rotations and two-qubit ZZ evolution gates. All gates here have Pauli rank $r_g = 1$ as discussed in Sec. A 1.

while we chose the cubically scaling Hamiltonian Fig. 2 (brown) as

$$\mathcal{H} = \sum_{k,l>m=1}^N J \sigma_x^{\{k\}} \sigma_y^{\{l\}} \sigma_z^{\{m\}} + \sum_{k=1}^N \omega_k \sigma_z^{\{k\}}. \quad (\text{A18})$$

In our simulations we start the optimisation at a random initial point in parameter space and let the system evolve until the gradient vector is such that $\|v\| = 10^{-1}$. We compute the values of N_F and N_g , and repeat this procedure 25 times. Dots (shading) [solid lines] Fig. 2 shows the average (standard deviation) [fitting] of the ratio N_F/N_g .

Appendix B: Propagating Variances

Lemma 2. *If the elements of \mathbf{F}_Q and \underline{g} are measured independently and their errors are sufficiently small, then the error measure can be written in the form*

$$\epsilon^2 = \sum_{k,l=1}^{\nu} a_{kl} \text{Var}\{[\mathbf{F}_Q]_{kl}\} + \sum_{k=1}^{\nu} b_k \text{Var}[g_l], \quad (\text{B1})$$

$$\text{where } a_{kl} := \sum_{i,j=1}^{\nu} [\mathbf{F}_Q^{-1}]_{ik}^2 [\mathbf{F}_Q^{-1}]_{lj}^2 g_l^2, \quad b_k := \sum_{l=1}^{\nu} \{[\mathbf{F}_Q^{-1}]_{kl}\}^2. \quad (\text{B2})$$

Proof. Under the assumption that the elements are measured independently and are sufficiently small, it is appropriate to use the variance formula [48], thus we can write error measure in terms of the variance of the elements in \mathbf{F}_Q^{-1} and \underline{g} yielding

$$\epsilon^2 = \sum_{k=1}^{\nu} \text{Var}[v_k] \quad (\text{B3})$$

$$= \sum_{k,l=1}^{\nu} \text{Var}\{[\mathbf{F}_Q^{-1}]_{kl}\} g_l^2 + \{[\mathbf{F}_Q^{-1}]_{kl}\}^2 \text{Var}[g_l]. \quad (\text{B4})$$

Now we use the result derived in [49] to relate the variance of elements of \mathbf{F}_Q^{-1} to elements of \mathbf{F}_Q , namely

$$\text{Var}\{[\mathbf{F}_Q]_{kl}^{-1}\} = \sum_{i,j=1}^{\nu} [\mathbf{F}_Q^{-1}]_{ik}^2 \text{Var}\{[\mathbf{F}_Q]_{kl}\} [\mathbf{F}_Q^{-1}]_{lj}^2. \quad (\text{B5})$$

Substituting this result into the error metric and trivially rearranging yields the required result

$$\epsilon^2 = \sum_{k,l=1}^{\nu} \left[\sum_{i,j=1}^{\nu} [\mathbf{F}_Q^{-1}]_{ik}^2 \text{Var}\{[\mathbf{F}_Q]_{kl}\} [\mathbf{F}_Q^{-1}]_{lj}^2 \right] g_l^2 + \{[\mathbf{F}_Q^{-1}]_{kl}\}^2 \text{Var}[g_l] \quad (\text{B6})$$

$$= \sum_{k,l=1}^{\nu} \underbrace{\left[\sum_{i,j=1}^{\nu} [\mathbf{F}_Q^{-1}]_{ik}^2 [\mathbf{F}_Q^{-1}]_{lj}^2 g_l^2 \right]}_{a_{kl}} \text{Var}\{[\mathbf{F}_Q]_{kl}\} + \sum_{k=1}^{\nu} \underbrace{\left[\sum_{l=1}^{\nu} \{[\mathbf{F}_Q^{-1}]_{kl}\}^2 \right]}_{b_k} \text{Var}[g_k]. \quad (\text{B7})$$

(B8)

□

1. Proof of Theorem 1

Proof. Recall that Lemma 2 establishes the error propagation formula which we abbreviate as $\epsilon^2 = \epsilon_F^2 + \epsilon_g^2$ via

$$\epsilon_F^2 := \sum_{\alpha,\beta=1}^{\nu} a_{\alpha\beta} \text{Var}\{[\mathbf{F}_Q]_{\alpha\beta}\}, \quad \epsilon_g^2 := \sum_{l=1}^{\nu} b_l \text{Var}[g_l]. \quad (\text{B9})$$

The coefficients $a_{\alpha\beta}$ can be upper bounded as

$$a_{\alpha\beta} = \sum_{k,l=1}^{\nu} g_l^2 [\mathbf{F}_Q^{-1}]_{k\alpha}^2 [\mathbf{F}_Q^{-1}]_{l\beta}^2 \leq \|g\|_{\infty}^2 \sum_{k=1}^{\nu} [\mathbf{F}_Q^{-1}]_{k\alpha}^2 \sum_{l=1}^{\nu} [\mathbf{F}_Q^{-1}]_{l\beta}^2, \quad \text{and} \quad b_l = \sum_{k=1}^{\nu} [\mathbf{F}_Q^{-1}]_{kl}^2,$$

where $\|g\|_{\infty}$ is the absolute largest element in the gradient vector. We assume that every matrix and vector element is assigned measurements uniformly as N_F/ν^2 and N_g/ν where N_F and N_g are the overall number of measurements required to estimate the matrix and vector objects such that the vector \underline{v} is obtained to a precision ϵ . Using the upper bounds on the variances of individual gradient vector entries from Eq. (A11) and individual matrix entries from Eq. (A15) and Eq. (A14) we derive the explicit bound

$$\text{Var}\{[\mathbf{F}_Q]_{\alpha\beta}\} \leq V_F := \nu^2 N_F^{-1} f_F \quad \text{Var}[g_l] \leq V_G := \nu N_g^{-1} \text{Spc}[\mathcal{H}] f_g,$$

where $\|\mathcal{H}\|$ is the Hilbert-Schmidt or Frobenius norm of the Hamiltonian and f_F, f_g are constant factors that depend on the ansatz structure and the and the approach used to estimate the gradient/Fisher matrix, refer to Sec. A 1. For example for the simplified ansatz in Sec. A 1 $f_F \leq 2$ and $f_g = 1$.

We use the above derived upper bounds and obtain

$$\epsilon_F^2 \leq V_F \|g\|_{\infty}^2 \sum_{\alpha,k=1}^{\nu} [\mathbf{F}_Q^{-1}]_{k\alpha}^2 \sum_{\beta,l=1}^{\nu} [\mathbf{F}_Q^{-1}]_{l\beta}^2 = V_F \|g\|_{\infty}^2 \|\mathbf{F}_Q^{-1}\|^4, \quad \epsilon_g^2 \leq V_G \sum_{k,l=1}^{\nu} [\mathbf{F}_Q^{-1}]_{kl}^2 = V_G \|\mathbf{F}_Q^{-1}\|^2, \quad (\text{B10})$$

where $\|\mathbf{F}_Q^{-1}\|$ is the Hilbert-Schmidt or Frobenius norm of the inverse matrix \mathbf{F}_Q^{-1} .

We now require that $\epsilon^2/2 =: \epsilon_F^2$ and $\epsilon^2/2 =: \epsilon_g^2$ as a possible choice to satisfy $\epsilon^2 = \epsilon_F^2 + \epsilon_g^2$. This results in the explicit bound on the number of measurements after substituting V_F and V_G as

$$N_F \leq 2 \nu^2 \|g\|_{\infty}^2 \|\mathbf{F}_Q^{-1}\|^4 \epsilon^{-2} f_F \quad N_g \leq 2 \nu \|\mathbf{F}_Q^{-1}\|^2 \epsilon^{-2} \text{Spc}[\mathcal{H}] f_g.$$

We introduce the notation $\text{Spc}[\mathbf{F}_Q^{-1}] := \|\mathbf{F}_Q^{-1}\|^2/\nu = \frac{1}{\nu} \sum_{k=1}^{\nu} \sigma_k^2(\mathbf{F}_Q^{-1})$ to denote the average of the squared singular values of \mathbf{F}_Q^{-1} . Note that, for example, the identity operator yields $\text{Spc}[\text{Id}] = 1$ and we derive upper and lower bounds on in general in Lemma 3.

We finally establish the upper bounds

$$N_F \leq 2 \nu^4 \|g\|_{\infty}^2 \text{Spc}[\mathbf{F}_Q^{-1}]^2 \epsilon^{-2} f_F, \quad N_g \leq 2 \nu^2 \text{Spc}[\mathbf{F}_Q^{-1}] \epsilon^{-2} \text{Spc}[\mathcal{H}] f_g.$$

□

2. Proof of Theorem 2

Proof. We use the limit $\mathbf{F}_Q^{-1} \rightarrow \text{Id}$ and $\text{Var}\{[\mathbf{F}_Q]_{kl}\} \rightarrow 0$ which straightforwardly recovers the sampling cost of the gradient vector as

$$N_g = N_{smp} := \sum_{l=1}^{\nu} \text{Var}[g_l].$$

Let us start by explicitly writing the ratio of measurements as

$$\frac{N_g}{N_{smp}} = \frac{\sum_{l=1}^{\nu} b_l \text{Var}[g_l]}{\sum_{l=1}^{\nu} \text{Var}[g_l]}$$

and let us consider the term

$$b_l = \sum_{k=1}^{\nu} [\mathbf{F}_Q^{-1}]_{kl}^2 = \|\text{Col}_l[\mathbf{F}_Q^{-1}]\|^2 = \|\mathbf{F}_Q^{-1} B_l\|^2 \leq \|\mathbf{F}_Q^{-1}\|_{\infty}^2 = \sigma_{\max}(\mathbf{F}_Q^{-1})^2 \leq \eta^{-2}$$

where η is either a regularisation parameter or the smallest singular value of \mathbf{F}_Q , $\text{Col}_l[\mathbf{F}_Q^{-1}]$ denotes the l -th column vector of the matrix \mathbf{F}_Q^{-1} and B_l is the l -th standard basis vector with $\|B_l\| = 1$. Our general upper bound follows as

$$\frac{N_g}{N_{smp}} = \frac{\sum_{l=1}^{\nu} b_l \text{Var}[g_l]}{\sum_{l=1}^{\nu} \text{Var}[g_l]} \leq \eta^{-2} \frac{\sum_{l=1}^{\nu} \text{Var}[g_l]}{\sum_{l=1}^{\nu} \text{Var}[g_l]} = \eta^{-2}$$

We now establish an approximation under the assumption that $\text{Var}[g_l]$ does not significantly depend on the index l , e.g., when the gradient is vanishing close to an optimal point via $M_{kl} \rightarrow 0$ in Eq. (A10) as

$$\text{Var}[g_k] = \sum_{l=1}^{r_h} h_l^2 (1 - [M_{kl}]^2) \rightarrow \sum_{l=1}^{r_h} h_l^2 = \text{Spc}[\mathcal{H}]. \quad (\text{B11})$$

This results in

$$\frac{N_g}{N_{smp}} = \frac{\sum_{l=1}^{\nu} b_l \text{Var}[g_l]}{\sum_{l=1}^{\nu} \text{Var}[g_l]} \approx \frac{\sum_{l=1}^{\nu} b_l}{\nu} = \frac{\sum_{k,l=1}^{\nu} [\mathbf{F}_Q^{-1}]_{kl}^2}{\nu} = \|\mathbf{F}_Q^{-1}\|/\nu = \text{Spc}[\mathbf{F}_Q^{-1}].$$

□

3. Remarks on Theorem 2

We establish bounds in case of the relative-precision scheme, i.e., when $\epsilon \propto \|g(t)\|$ and $\epsilon \propto \|v(t)\|$ in case of the gradient and natural gradient vectors, respectively. The upper bound follows via

$$\frac{\|g\|^2}{\|v\|^2} = \frac{\|g\|^2}{\|\mathbf{F}_Q^{-1} g\|^2} \leq \sigma_{\min}(\mathbf{F}_Q^{-1})^{-2}, \quad (\text{B12})$$

and a lower bound can be specified as

$$\frac{\|g\|^2}{\|v\|^2} = \frac{\|g\|^2}{\|\mathbf{F}_Q^{-1} g\|^2} \geq \sigma_{\max}(\mathbf{F}_Q^{-1})^{-2} \quad (\text{B13})$$

and in complete generality

$$\frac{N_g}{N_{smp}} \frac{\|g\|^2}{\|v\|^2} \leq [\sigma_{\max}(\mathbf{F}_Q^{-1})/\sigma_{\min}(\mathbf{F}_Q^{-1})]^2 =: \text{Cnd}[\mathbf{F}_Q^{-1}]^2, \quad (\text{B14})$$

and Lemma 3 establishes that $\text{Cnd}[\mathbf{F}_Q^{-1}] \leq \eta^{-1}(\nu r_g + \eta)$.

Lemma 3. Assuming the simple regularisation $\mathbf{F}_Q^{-1} := (\mathbf{F}_Q + \eta \text{Id}_\nu)^{-1}$, the largest singular value of the inverse is upper bounded as $\sigma_{\max}(\mathbf{F}_Q^{-1}) \leq \eta^{-1}$ and the smallest singular value is lower bounded via $\sigma_{\min}(\mathbf{F}_Q^{-1}) \geq (\nu r_g + \eta)^{-1}$. Moreover, the bounds $(\nu r_g + \eta)^{-2} \leq \text{Spc}[\mathbf{F}_Q^{-1}] \leq \eta^{-2}$ and $\text{Cnd}[\mathbf{F}_Q^{-1}] \leq \eta^{-1}(\nu r_g + \eta)$ hold in general. Here r_g is the largest Pauli rank of the ansatz gates from Sec. A 1.

Proof. Using that \mathbf{F}_Q is positive semi-definite, it trivially follows that

$$\sigma_{\max}([\mathbf{F}_Q + \eta \text{Id}_\nu]^{-1}) = [\sigma_{\min}(\mathbf{F}_Q + \eta \text{Id}_\nu)]^{-1} \leq \eta^{-1}$$

via $\sigma_{\min}(\mathbf{F}_Q + \eta \text{Id}_\nu) \geq \eta$. Now we use the boundedness of the matrix elements as $|[\mathbf{F}_Q^{-1}]_{kl}| \leq r_g^2$ from Lemma 1 which establishes the matrix norm $\|\mathbf{F}_Q\|_{\max} := \max_{k,l} |[\mathbf{F}_Q]_{kl}| \leq r_g^2$. This bounds the largest singular value of \mathbf{F}_Q as

$$r_g^2 \geq \|\mathbf{F}_Q\|_{\max} \geq \|\mathbf{F}_Q\|_\infty/\nu := \sigma_{\max}(\mathbf{F}_Q)/\nu.$$

The smallest singular value of the inverse is therefore bounded as

$$\sigma_{\min}([\mathbf{F}_Q + \eta \text{Id}_\nu]^{-1}) = [\sigma_{\max}(\mathbf{F}_Q + \eta \text{Id}_\nu)]^{-1} \geq (\nu r_g^2 + \eta)^{-1}.$$

We can now establish the bound

$$(\nu r_g^2 + \eta)^{-2} \leq \sigma_{\min}^2(\mathbf{F}_Q^{-1}) \leq \text{Spc}[\mathbf{F}_Q^{-1}] \leq \sigma_{\max}^2(\mathbf{F}_Q^{-1}) \leq \eta^{-2} \quad (\text{B15})$$

And we can therefore bound the growth rate of the quantity $\text{Spc}[\mathbf{F}_Q^{-1}]$ as $\text{Spc}[\mathbf{F}_Q^{-1}] = \mathcal{O}(\nu^s)$ with $-2 \leq s \leq 0$. \square

Appendix C: Optimal Measurements

Lemma 4. Measurements are distributed optimally when the number of samples for determining individual elements of the matrix and gradient are given by

$$[\mathbf{N}_F]_{kl} = \epsilon^{-2} \Sigma \sqrt{a_{kl} \text{Var}\{[\mathbf{F}_Q]_{kl}\}}, \quad (\text{C1})$$

$$[\mathbf{N}_g]_k = \epsilon^{-2} \Sigma \sqrt{b_k \text{Var}[g_k]}, \quad (\text{C2})$$

respectively. Here $\text{Var}[\cdot]$ is the variance of a single measurement of the corresponding element and we explicitly define Σ via the coefficients a_{kl} and b_k from Appendix B as

$$\Sigma := \sum_{k,l=1}^{\nu} \sqrt{a_{kl} \text{Var}\{[\mathbf{F}_Q]_{kl}\}} + \sum_{k=1}^{\nu} \sqrt{b_k \text{Var}[g_k]}. \quad (\text{C3})$$

Proof. From Lemma 2 we write the error measure as

$$\epsilon^2 = \sum_{k,l=1}^{\nu} a_{kl} \text{Var}\{[\mathbf{F}_Q]_{kl}\} + \sum_{k=1}^{\nu} b_k \text{Var}[g_k], \quad (\text{C4})$$

where $\text{Var}[\cdot]$ denotes the variance in the statistical average over many measurements. Now we allow $\text{Var}[\cdot]$ to denote variance in a single measurement while $[\mathbf{N}_F]_{kl}$ and $[\mathbf{N}_g]_k$ are the number of measurement assigned each element $[\mathbf{F}_Q]_{kl}$ and g_k respectively, so the error measure becomes

$$\epsilon^2 = \sum_{k,l=1}^{\nu} \frac{a_{kl} \text{Var}\{[\mathbf{F}_Q]_{kl}\}}{[\mathbf{N}_F]_{kl}} + \sum_{k=1}^{\nu} \frac{b_k \text{Var}[g_k]}{[\mathbf{N}_g]_k}. \quad (\text{C5})$$

By minimising error measure, in this form, subject to the constraint of a fixed total number of measurements, so that

$$N_{opt} = \sum_{k,l=1}^{\nu} [\mathbf{N}_F]_{kl} + \sum_{k=1}^{\nu} [\mathbf{N}_g]_k, \quad (\text{C6})$$

we find that the optimal fraction of measurement to be assigned to each element is

$$\frac{[\mathbf{N}_F]_{kl}}{N_{\text{opt}}} = \frac{\sqrt{a_{kl} \text{Var}\{[\mathbf{F}_Q]_{kl}\}}}{\Sigma}, \quad \frac{[\mathbf{N}_g]_k}{N_{\text{opt}}} = \frac{\sqrt{b_k \text{Var}[g_k]}}{\Sigma} \quad (\text{C7})$$

$$\text{where } \Sigma := \sum_{k,l=1}^{\nu} \sqrt{a_{kl} \text{Var}\{[\mathbf{F}_Q]_{kl}\}} + \sum_{k=1}^{\nu} \sqrt{b_k \text{Var}[g_k]}. \quad (\text{C8})$$

By substituting this results in the error measure we can remove the dependence on the total number of measurements N_{opt} , to yield the required result. \square

1. Fisher Matrix Symmetry

Lemma 5. *The symmetry of Fisher Matrix can be accounted for by replacing the elements a_{kl} with a'_{kl} , where*

$$a'_{kl} := \begin{cases} 0 & k < l \\ a_{kk} & k = l \\ a_{kl} + a_{lk} & k > l \end{cases} \quad (\text{C9})$$

Proof. As the Fisher Matrix is symmetric, measurements of $[\mathbf{F}_Q]_{kl}$ element also constitute measurements of the $[\mathbf{F}_Q]_{lk}$, so $\text{Var}\{[\mathbf{F}_Q]_{kl}\} = \text{Var}\{[\mathbf{F}_Q]_{lk}\}$. Thus, the error measure can be written as

$$\epsilon^2 = \sum_{k=1}^{\nu} a_{kk} \text{Var}\{[\mathbf{F}_Q]_{kk}\} + \sum_{k>l}^{\nu} 2a_{kl} \text{Var}\{[\mathbf{F}_Q]_{kl}\} + \sum_{k=1}^{\nu} b_k \text{Var}[g_k]. \quad (\text{C10})$$

It is possible to force this back into the original form of the error measure if we define

$$a'_{kl} := \begin{cases} 0 & k < l \\ a_{kk} & k = l \\ a_{kl} + a_{lk} & k > l \end{cases}, \quad (\text{C11})$$

so that the error measure error measure can be written as

$$\epsilon^2 = \sum_{k,l=1}^{\nu} a'_{kl} \text{Var}\{[\mathbf{F}_Q]_{kl}\} + \sum_{k=1}^{\nu} b_k \text{Var}[g_k]. \quad (\text{C12})$$

Using the error measure written in this form as a starting point for the derivation in the proof of Lemma 4 we trivially obtain the same results with the elements a_{kl} replaced with a'_{kl} . \square